Unraveling the $LiNbO_3$ X-cut surface by atomic force microscopy and density functional theory

S. Sanna* and W. G. Schmidt
Lehrstuhl für Theoretische Physik, Universität Paderborn, 33095 Paderborn, Germany

S. Rode,† S. Klassen, and A. Kühnle
Institut für Physikalische Chemie, Fachbereich Chemie, Johannes Gutenberg-Universität Mainz, Duesbergweg 10-14, 55099 Mainz, Germany
(Received 28 November 2013; revised manuscript received 23 January 2014; published 7 February 2014; corrected 12 March 2014)

The $LiNbO_3(2\bar{1}\bar{1}0)$ surface, commonly referred to as X-cut, is investigated by means of atomic force microscopy and first-principles calculations. Atomically resolved atomic force microscopy images show geometrical patterns not compatible with truncated bulk terminations. Fast Fourier transformation of the real-space images shows an oblique surface unit cell with lattice parameters of $a = 0.75 \pm 0.02$ nm, $b = 0.54 \pm 0.02$ nm, and $\alpha = 94.8°$. Comparing these experimental results with the theoretical models of stable surface terminations provides clear evidence for the formation of a -Li_{12} termination. The LN X-cut is, thus, characterized by a nonstoichiometric and Li-enriched composition. An analysis of the surface electronic charge indicates that the atomic force microscopy contrast is governed by the charge accumulation at the oxygen ions.

DOI: 10.1103/PhysRevB.89.075403 PACS number(s): 68.35.B−, 68.37.Ps, 68.47.Gh, 77.84.−s

I. INTRODUCTION

$LiNbO_3$ (LN) is a manmade ferroelectric crystal with outstanding electro-optical properties [1]. The vast majority of LN applications exploit the bulk characteristics of the material. However, LN surfaces are of great technological relevance as well. Among the LN surfaces employed in technologic applications, the LN$(2\bar{1}\bar{1}0)$ is the only surface which is neither polar nor piezoelectric. This surface, commonly referred to as LN X-cut, is particularly suitable as a substrate for the deposition of the stoichiometric LN thin films [2] required for applications in integrated optics. Furthermore, it is largely employed for the realization of surface acoustic wave devices [3] and X-cut optical waveguides [4]. Despite many exciting applications, little detailed information on the morphology of the LN$(2\bar{1}\bar{1}0)$ is available. Lee has investigated rough surfaces of commercial X-cut substrates by atomic force microscopy, showing that they can be smoothed on atomic scale simply by annealing in air [5]. Nagata has demonstrated that the ion concentration of the unintentional dopant hydroxyl changes along the z axis in X-cut wafers [6]. It remains, however, unclear whether the concentration gradient is a surface or subsurface characteristic of the samples. Bentini *et al.* [7] have investigated ion implanted X-cut LN single crystals by secondary ion mass spectrometry, Rutherford back-scattering spectroscopy, and x-ray diffraction. No surface damage has been detected for carbon implantation at low fluency. The main effect of the implantation at the surface has been described as the appearance of tensile strain and corresponding enlargement of the lattice unit cell. Similarly, Kalabin *et al.* have not observed the formation of any new phase upon Ti indiffusion and annealing [8]. However, no experimental information is available so far regarding the X-cut surface structure at the atomic scale. Neither is it known whether the LN X-cut reconstructs or not, as no high-resolution images of the surface are available. On the other hand, microscopic models of the thermodynamically stable (1×1) surface terminations have been theoretically predicted recently [9]. According to the proposed models, X-cut surfaces are Li-enriched with respect to the LN bulk. Indeed a -Li_{12} termination has been found to be formed under most growth conditions. It represents the X-cut surface with the lowest work function and the lowest surface-induced dipole moment [9]. Nevertheless, other stable terminations, such as a relaxed truncated bulk -Li_6Nb_6-O_9, and -Li_9 (for very O-rich conditions) may also occur, according to the calculations.

In this work, we present a combined investigation of the LN$(2\bar{1}\bar{1}0)$ by frequency-modulated atomic force microscopy (FM-AFM) and density functional theory (DFT). Real-space images are obtained, revealing atomic resolution of the LN X-cut. No differences between the +X and the −X surface are observed. The atomically resolved AFM images are compared to the charge distributions obtained from the DFT models. From this comparison, we assign the -Li_{12} model to the X-cut seen in AFM. The measured oblique pattern with lattice parameters of $a = 0.75 \pm 0.02$ nm, $b = 0.54 \pm 0.02$ nm, and $\alpha = 94.85°$ observed in the AFM images can be readily assigned to the outermost oxygen layer.

II. EXPERIMENT

All investigated samples are commercially available X-cut wafers (99-00629-01, Crystal Technology, Inc., USA). Before inserting into the AFM, the samples were cut into 1×1 cm^2 pieces and cleaned in acetone and isopropanol in an ultrasonic bath for 15 min each. After cleaning, the samples were dried in a nitrogen flow and annealed at different temperatures for 5 h in a muffle furnace from Nabertherm GmbH (Lilienthal, Germany). For the high-resolution images shown in Fig. 4, the samples were annealed for 10 h at a temperature of 900 or 1000 °C. All samples were allowed to equilibrate to room temperature after annealing.

Large-scale images were taken using standard tapping mode AFM (Bruker Multimode AFM) in air. All atomic-resolution FM-AFM images were obtained in Milli-Q water (Millipore GmbH, Schwalbach, Germany) using a specifically

*simone.sanna@uni-paderborn.de
†Now at SmarAct GmbH.

optimized instrument for atomic-resolution imaging in liquids (deflection spectral noise density of below 10 fm/$\sqrt{\text{Hz}}$) [10]. As force sensors, we used gold-coated, *p*-doped silicon cantilevers (PPP-NCHAuD from Nanosensors, Neuchâtel, Switzerland) with an eigenfrequency of about 160 kHz, a spring constant of about 40 N/m, and a Q value of around 8 in Milli-Q water. The cantilever oscillation amplitude was kept constant at a level of around $A \approx 0.5$–1.5 nm. The atomically resolved experiments were repeated five (three) times for the positive (negative) X-cut. Care was taken not to contaminate the surface by using ultrasound-cleaned equipment.

III. THEORY

First-principles total-energy calculations within the DFT as implemented in VASP [11] are performed using the projector-augmented wave method [12]. The generalized gradient approximation of the exchange-correlation functional in its PW91 formulation [13], plane-wave expansions up to 400 eV, and projectors up to $l = 3$ for Nb and $l = 2$ for Li and O were used for all the calculations. A Monkhorst-Pack $1 \times 2 \times 2$ k-point mesh [14] was used to carry out the integration in the Brillouin zone of the slabs described in the following. This approach is, thus, equivalent to the approach adopted in our previous works [15,16]. It has been demonstrated to yield reliable structures and energies for both LN bulk and surfaces [17].

$LiNbO_3$ is usually modeled by a rhombohedral or a hexagonal unit cell, containing 10 and 30 atoms, respectively. Unfortunately, neither the hexagonal nor the rhombohedral unit cell have faces parallel to the LN X-cut and are, therefore, not suited for the simulation of this surface. The smallest unit cell with a face parallel to the $(2\bar{1}\bar{1}0)$ is an orthogonal cell containing 60 atoms (12 formula units). This cell represents the starting point for the modeling of the LN X-cut in this work. Following the approach described in Ref. [9], we double the orthogonal unit cell along the x direction, so that the slabs used to model the X-cut consist of 120 atoms plus the surface termination, and a vacuum region of about 11 Å in height above the slab. The atomic positions of the first nine layers were kept fixed at their bulk values. The outer three and all the termination layers in the slab unit cell were allowed to relax freely, until the Hellmann-Feynman forces become lower than 0.02 eV/Å. As the ions of the lower part of the slab were kept frozen at their bulk positions and the atoms of the upper part were used to model the different terminations, the slab is characterized by two nonequivalent surface terminations. Different surface terminations give rise to a net dipole moment perpendicular to the surface. Thus, the surface will be affected by the artificial field caused by its neighboring periodic images. In order to correct for the error introduced by the artificial field in finite slabs, dipole corrections were applied [18]. The correction consists of an external dipole layer in the vacuum region of the supercell [19].

As no other surface periodicity than the (1×1) at the X-cut has been reported in the literature [8], surface reconstructions are not considered in this work. We do, however, consider changes in morphology and stoichiometry within the (1×1) unit cell. Similarly, as there is no experimental evidence of LN surfaces with net spin moment, we restrict ourselves to spin-unpolarized calculations. Our models represent *clean* surfaces of *stoichiometric* LN. In congruent material the outgassing of LiO already at moderate temperatures (≈450 °C) might severely deteriorate the crystalline quality and affect the surface composition. However, this is not the case for the stoichiometric material.

The surface calculations used here for the interpretation of the AFM measurements model the stable surface terminations in equilibrium with a reservoir of Li, Nb, and O atoms at conditions specified by their chemical potentials (see Ref. [9]). While the presence of water may affect the relative stability of different surface terminations, it will not modify the range of the Li, Nb, and O chemical potentials that lead to stable LN surfaces. Moreover, as far as we know there is neither experimental nor theoretical evidence of a new, water-induced, termination or reconstruction at any lithium niobate surface. Therefore the surface structures found stable theoretically in Ref. [9] are at least a good starting point for the interpretation of the present AFM images. Furthermore, it has been recently shown that the presence of water on $LiNbO_3(0001)$ slightly accentuates the surface relaxation, but does not drastically

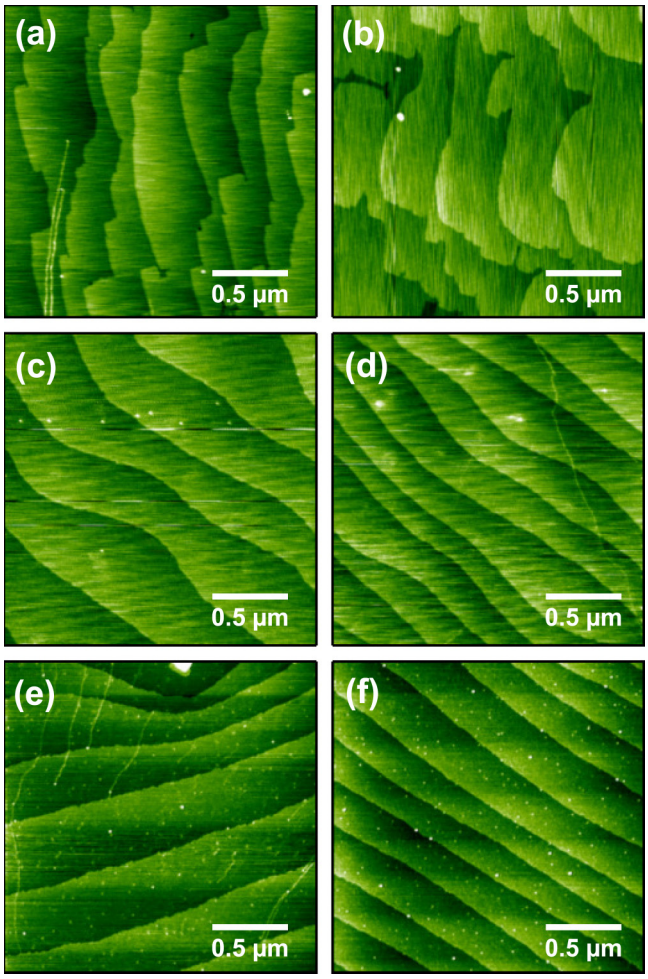

FIG. 1. (Color online) Tapping mode AFM images of the positive (left-hand side) and negative (right-hand side) LN X-cut at the μm scale. Images were taken in air after cleaning in acetone and isopropanol in an ultrasonic bath and annealing at 700 °C [(a) and (b)], 800 °C [(c) and (d)], and 900 °C [(e) and (f)].

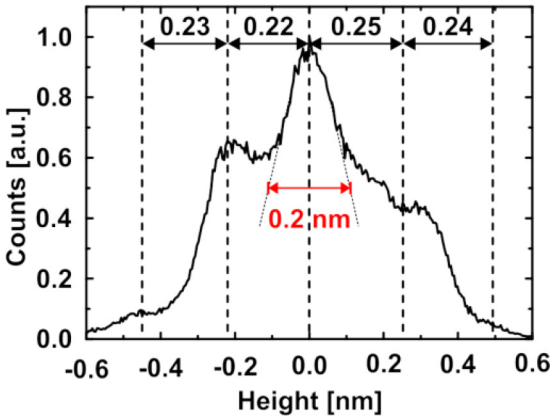

FIG. 2. (Color online) Height distribution plot at the LN($2\bar{1}\bar{1}0$) surface. The distribution originates from an area of 1 μm^2. The corresponding sample was cleaned in acetone and isopropanol in an ultrasonic bath for 15 min each, dried in a nitrogen flow, and annealed at 1000 °C for 10 h.

affect the surface morphology (see Ref. [17]). In the same work, it was shown that AFM measurements in aqueous solution do not image the water film at the surface but the surface itself.

IV. RESULTS

Micrometer-scale AFM images of the X-cut surfaces taken in air are presented in Fig. 1. These images illustrate the dependence of the surface morphology on the annealing temperature in the range 700–900 °C. A step structure consisting of regular, flat terraces can be observed. The presence of the terraces is due to a cut angle not perfectly perpendicular to the x axis. We evaluate the step height by means of a height distribution plot as shown in Fig. 2. Such a height distribution plot provides the advantage of averaging the measurement over a large area, thus, an accurate estimate of the step height is achieved. The measured value of 0.24 ± 0.2 nm is in excellent agreement with previous measurements as compiled in Table I. The measured value is very close to the distance between

TABLE I. Measured step height of the terraces on the LN X-cut. Available data as well as theoretical predictions are compiled for comparison.

Anneal	Height (nm)	Ref.
800 °C	0.24 ± 0.2	This work
–	0.28	[20]
980 °C	0.24	[8][a]
1000 °C	0.45 ± 0.04	[5][b]
–	0.26	Atomic layer distance in bulk
–	0.23	Atomic layer distance at the surface.[c]

[a]Minimum measured step height. In this work, strong precipitation of $HNbO_3$ accompanied by $LiNb_3O_8$ formation after annealing above 900 °C has been observed.

[b]The deviation from other results is probably due to a different notation concerning atomic planes.

[c]Distance between first and second atomic layers according to the -Li_{12} surface model as proposed in Ref. [9].

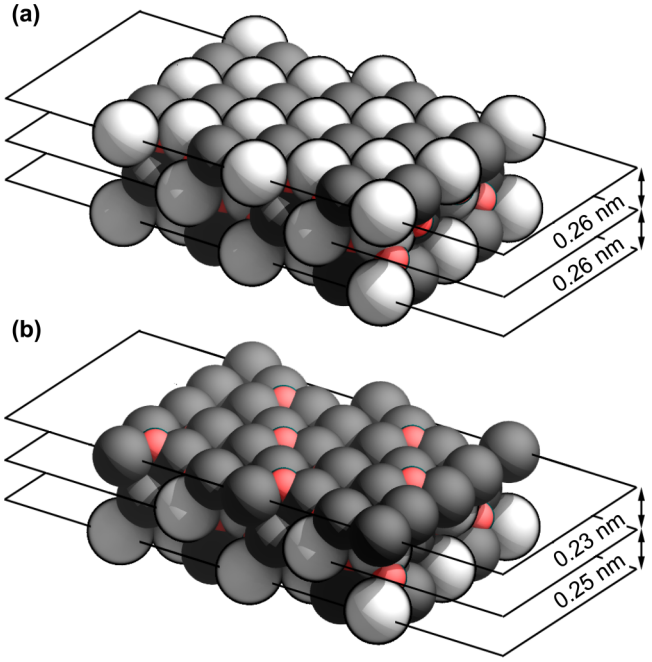

FIG. 3. (Color online) Perspective view of (a) the unrelaxed truncated-bulk X-cut and (b) the -Li_{12} terminated X-cut. Distances between the atomic layers are indicated. White atoms represent Nb, gray atoms Li, and small atoms O.

consecutive cationic planes in bulk LN shown in Fig. 3(a). The deviation from the bulk value can be explained by relaxation phenomena at the surface. Indeed, the distance between first and second atomic layers in the -Li_{12} surface termination proposed in Ref. [9] and shown in Fig. 3(b) is 0.23 nm, a value very close to the measured one. As expected, the +X and −X surfaces do not show appreciable differences. Indeed, differently from the y and z directions, the x axis is perpendicular to a plane of mirror symmetry. Thus, while +Z and −Z cuts as well as +Y and −Y cuts are intrinsically different (as seen, e.g., in etching rates, chemical reactivity, etc.), the +X and −X cuts are completely equivalent.

Figure 4 shows an atomically resolved FM-AFM image of the LN X-cut surface. The pictures represent the positive face after annealing at 900 °C, i.e., the sample presented in Fig. 1(e). As shown, true atomic resolution is achieved, which allows for determining the surface unit cell by fast Fourier

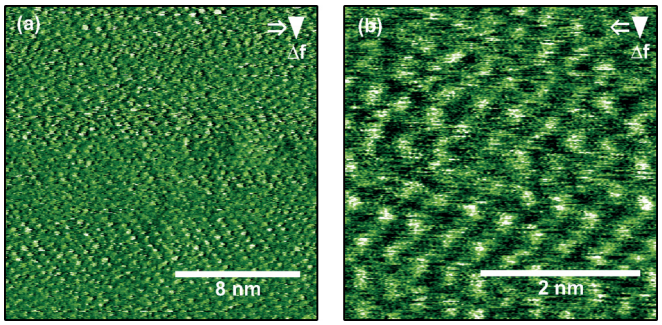

FIG. 4. (Color online) High-resolution FM-AFM images of the positive X-cut sample shown in Fig. 1(e).

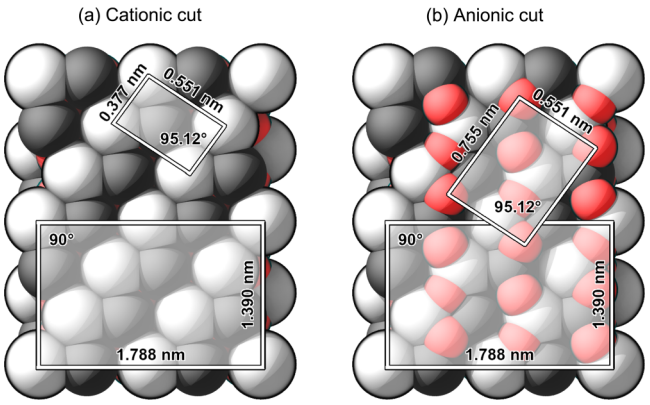

FIG. 5. (Color online) Atomic models of the truncated bulk terminations of the LN X-cut. Two nonequivalent cuts with (a) cationic and (b) anionic terminations can be discriminated. White atoms represent Nb, gray atoms Li, and small atoms O. The unit cells of arbitrarily chosen surface atoms are highlighted. Note that all the Li and Nb ions, as well as all the oxygen ions, are located at the same height.

transformation (FFT). To determine the unit cell structure and dimensions with high accuracy, it is necessary to correct for the linear drift. The drift correction was performed by averaging the FFT of several subsequent images, taken in a series of upward and downward scans. To benefit from further error cancelation, we collected also a forward and a backward scan for each image set and then averaged both upward and downward as well as forward and backward images. The back transformation of the averaged FFT representation reveals the drift-corrected real-space dimensions of the surface unit cell. The unit cell is oblique with lattice constants $a = 0.75 \pm 0.02$ nm, $b = 0.54 \pm 0.02$ nm, and $\alpha = 94.8^\circ$ These values do not correspond to the truncated bulk models, as outlined in the following. Thus, our experimental results suggest the occurrence of surface phenomena such as relaxation or reconstructions.

Bulk LN can be considered as a stacking of cationic Li_6Nb_6 and anionic O_9 atomic layers in the x direction. The truncated bulk surface can, thus, either show a cationic [Fig. 5(a)] or anionic termination [Fig. 5(b)]. The unit cell of the cationic cut is an oblique cell with lattice constants of $a = 0.551$ nm and $b = 0.377$ nm. The unit cell extrapolated from the FFT of the AFM images is twice as large and could then be interpreted as a periodicity doubling in the pattern described by the outmost Li (or Nb) ions in a cationic cut shown Fig. 5(a). The anionic cut is characterized by nine nonequivalent oxygen sites at the same height. Again, the unit cell extrapolated from the FFT of the AFM images is not compatible with the oxygen pattern. The experimentally observed pattern could only be formed by a peculiar rearrangement raising four oxygen ions above the other, as indicated in Fig. 5(b). However, the supercell obtained from the FFT analysis might also be related to a nonstoichiometric termination.

Indeed, it is known from atomistic simulations that the LN X-cut is stabilized by modifications in morphology and stoichiometry. According to the calculations of Ref. [9], three

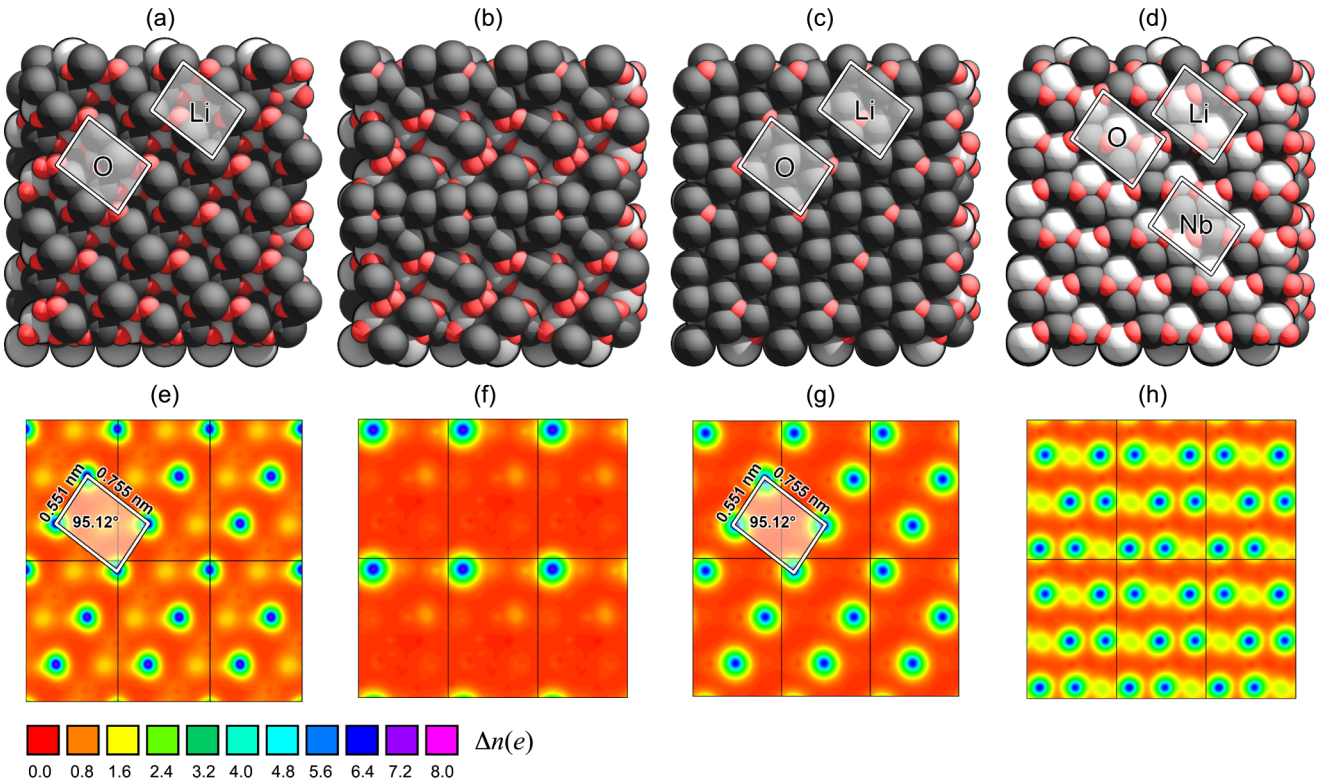

FIG. 6. (Color online) Calculated atomic models of the (a) -Li_6, (b) -Li_9, (c) -Li_{12}, and (d) $Li_6Nb_6O_9$ terminations. Atomic patterns compatible with the AFM pictures are highlighted. Color coding as in previous pictures. (e)–(h) Corresponding electronic charge distribution calculated 0.25 Å above the highest atom. The dimensions and the character of the surface unit cells as they would appear in AFM measurements are indicated.

different (1×1) surface terminations are thermodynamically stable, namely the -Li_6, -Li_{12}, and -$Li_6Nb_6O_9$ terminations. The latter corresponds to a relaxed truncated bulk. The Li-enriched terminations -Li_6, -Li_9 and -Li_{12} as well as the stoichiometric -$Li_6Nb_6O_9$ termination are shown in Figs. 6(a)–6(d).

The -Li_6 [Fig. 6(a)] and the -Li_{12} [Fig. 6(c)] are characterized by the emergence of bulk oxygen ions at the surface as a consequence of the surface relaxation. For both terminations, the surface oxygen describes an oblique 0.55 nm × 0.76 nm pattern. Both terminations are, therefore, compatible with the AFM data. Furthermore, the buckling of the surface Li causes the separation of the Li-layer in two sublayers. Also the topmost Li layer describes a pattern compatible with the AFM data. However, the first and second Li layers are separated by a vertical distance smaller than 0.01 nm, which can hardly result in the measured AFM pattern. The Li and O surface structures that would be in agreement with the experimental data are highlighted in Figs. 6(a) and 6(c).

The -Li_9 termination [Fig. 6(b)] does not show any surface structure compatible with the AFM images and will not be further discussed. The -$Li_6Nb_6O_9$ termination [Fig. 6(d)] corresponds to the relaxed anionic cut shown in Fig. 6(b). The surface relaxation causes a buckling of the surface atoms. As a result, the oxygen, the lithium, and also niobium sublattice would describe a pattern compatible with the experimental data. The Li, Nb and O surface structures that would be in agreement with the experimental data are highlighted in Fig. 6(d). From this analysis, we can unambiguously exclude the -Li_9 termination as possible surface structure mapped by the AFM measurements. It remains, however, open at this point as to which of the three remaining terminations is observed experimentally.

To understand the origin of the AFM pattern and, thus, discern which of the three remaining terminations is observed in the measured samples, we calculate the electronic charge distribution associated to the models of Figs. 6(a)–6(d). This greatly facilitates the interpretation of the AFM pictures, when assuming that the interaction between surface and AFM tip is related to the surface charge. The results of the calculation are shown in Figs. 6(e)–6(h). These data show that regions of higher charge density correspond to superficial oxygen ions. Due to their high electronegativity, these atoms tend to attract electronic charge in their neighborhood, resulting in a high contrast in the AFM images. Second, only the charge distribution associated with the -Li_6 and -Li_{12} terminations results in a pattern compatible with the AFM measurements. However, the -Li_6 termination is not thermodynamically stable, as it does not appear in the X-cut surface phase diagram.

The surface charge density of the -Li_{12} model, on the other hand, agrees very nicely with the measured AFM image, as shown in Fig. 7. This is a strong indication that the measured X-cut samples are -Li_{12} terminated. The surface oxygen ions describe the oblique pattern with dimensions of 0.76 nm × 0.55 nm, and $\alpha = 95.12^\circ$ as shown Fig. 6(g). These dimensions are in excellent agreement with the experimental results. The -Li_{12} surface mapped by AFM is the dominant termination in the X-cut phase diagram, and it is formed under most growth conditions. It has been found that this termination minimizes the surface work function as well as the surface induced dipole moment of LN X-cut samples [9].

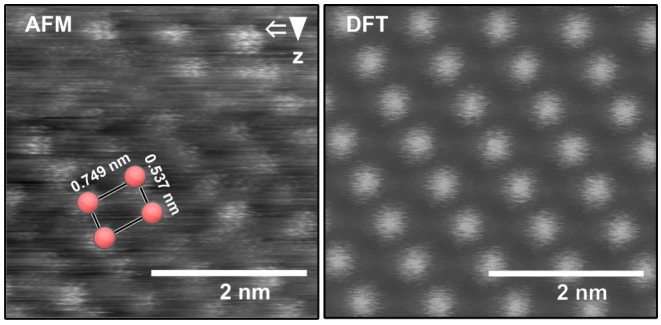

FIG. 7. (Color online) Comparison of the atomically resolved FM-AFM image of the LN X-cut (left-hand side) with the surface electronic charge density of the -Li_{12} terminated X-cut model calculated within the DFT (right-hand side). The bright spots in the pictures correspond to oxygen ions.

V. CONCLUSIONS

The $LiNbO_3$ $(2\bar{1}\bar{1}0)$ surface, commonly referred to as LN X-cut, was investigated by means of atomic force microscopy and density functional theory. Atomic resolved AFM pictures were obtained. The fast Fourier transformation of the real-space images lead to the identification of a 0.75 ± 0.02 nm $\times$ 0.54 ± 0.02 nm oblique surface pattern. The theoretical analysis of the structural models and corresponding electronic charge density of several X-cut terminations strongly suggest that (i) the observed AFM pattern can be ascribed to oxygen ions and (ii) the surface mapped by the AFM tip corresponds to the -Li_{12} terminated LN X-cut. The first point is a characteristic of all the investigated $LiNbO_3$ cuts and may be a common feature of the surfaces of other ionic compounds.

ACKNOWLEDGMENTS

The German Research Society (DFG) is acknowledged for financial support. All the calculations were performed at the Paderborn Center for Parallel Computing (PC^2) and at the High Performance Computing Center in Stuttgart (HLRS).

[1] R. S. Weis and T. K. Gaylord, Appl. Phys. Solid Surface **37**, 191 (1985).
[2] J. Kräußlich, C. Dubs, A. Lorenz, and A. Tünnermann, Phys. Status Solidi A **204**, 2585 (2007).
[3] T.-C. Lee, J.-T. Lee, M. A. Robert, S. Wang, and T. A. Rabson, Appl. Phys. Lett. **82**, 191 (2003).
[4] G. G. Bentini, M. Bianconi, M. Chiarini, L. Correra, C. Sada, P. Mazzoldi, N. Argiolas, M. Bazzan, and R. Guzzi, J. Appl. Phys. **92**, 6477 (2002).

[5] G. Lee, Opt. Express **10**, 556 (2002).
[6] H. Nagata, Opt. Eng. **37**, 1612 (1998).
[7] G. G. Bentini, M. Bianconi, A. Cerutti, M. Chiarini, G. Pennestrì, C. Sada, N. Argiolas, M. Bazzan, P. Mazzoldi, and R. Guzzi, Nucl. Instrum. Methods Phys. Res., Sect. B **240**, 174 (2005).
[8] I. Kalabin, T. Grigorieva, L. Pokrovsky, D. Sheglov, D. Shevtsov, and V. Atuchin, Opt. Commun. **221**, 359 (2003).
[9] S. Sanna and W. G. Schmidt, Phys. Rev. B **81**, 214116 (2010).
[10] S. Rode, R. Stark, J. Lübbe, L. Tröger, J. Schütte, K. Umeda, K. Kobayashi, H. Yamada, and A. Kühnle, Rev. Sci. Instrum. **82**, 073703 (2011).
[11] G. Kresse and J. Furthmüller, Phys. Rev. B **54**, 11169 (1996).
[12] P. E. Blöchl, Phys. Rev. B **50**, 17953 (1994).
[13] J. P. Perdew and Y. Wang, Phys. Rev. B **33**, 8800 (1986).
[14] H. J. Monkhorst and J. D. Pack, Phys. Rev. B **13**, 5188 (1976).
[15] S. Rode, R. Hölscher, S. Sanna, S. Klassen, K. Kobayashi, H. Yamada, W. G. Schmidt, and A. Kühnle, Phys. Rev. B **86**, 075468 (2012).
[16] S. Sanna, A. V. Gavrilenko, and W. G. Schmidt, Physica Status Solidi C **7**, 145 (2010).
[17] S. Sanna, R. Hölscher, and W. G. Schmidt, Phys. Rev. B **86**, 205407 (2012).
[18] J. Neugebauer and M. Scheffler, Phys. Rev. B **46**, 16067 (1992).
[19] L. Bengtsson, Phys. Rev. B **59**, 12301 (1999).
[20] *Properties of Lithium Niobate*, edited by K. K. Wong, EMIS Datareview Series No. 28 (Institution of Electrical Engineers, London, 2002).